Additive impact on early-stage magnesium carbonate mineralisation

F. Santoro De Vico, S. Bonilla-Correa, G. Pelayo-Punzano, K. Elert, C. Rodríguez-Navarro, E. Ruiz-Agudo

Supplementary Information

The Supplementary Information includes:

- Methodology
- Figures S-1 to S-6
- Table S-1
- Supplementary Information References

Methodology

In situ monitoring of $MgCO_3$ precipitation.

$MgCO_3$ precipitation experiments were carried out at a fixed pH of 11, maintained by NaOH addition using a Titrino 905 (Methrom). A 100 mM magnesium chloride (Sigma Aldrich, anhydrous, ≥98 %) solution was continuously added at a rate of 0.12 mL min^{-1} to a 50 mM potassium carbonate (Sigma Aldrich, anhydrous, free-flowing, Redi-Dri™, ACS reagent, ≥99 %) buffer. Tri-sodium citrate dihydrate (Sigma Aldrich, ACS, ISO, Reag. Ph Eur; 0.04 to 5 mM) was added to the carbonate buffer. Each titration experiment was performed at least in triplicate (10 times for runs without additives) for representativity. pH, solution conductivity and transmittance were monitored during the duration of the experiments using a glass electrode, a conductometric cell and a photometric sensor equipped with a laser at a wavelength of 610 nm by Metrohm, respectively. The cell constant of the conductivity probe was determined by measurement of an electrolyte solution with known conductivity (in this case, 0.01 and 0.1 M potassium chloride standard solutions, with a conductivity of 1.41 mS/cm and 12.88 mS/cm, respectively). *In situ*, continuous monitoring of the evolution of particle size evolution was performed by dynamic light scattering (DLS), using a Microtrac NANO-flex analyzer. The system consists of a 780 nm diode laser with 5 mW power and a probe with sapphire window and a length of 1 m and diameter of 8 mm. Each run was acquired during 45 s, with an elapsed time between measurements of 20 s. The Microtrac FLEX software (v.11.1.0.1) was used for determination of particle size distributions. Finally, we performed zeta potential analysis of AMC samples using a Microtrac Zeta-check particle charge analyser. 3 mL of the reaction media were taken directly from the reactor of the titration system in two different points of the transmittance curve (immediately after the first drop of the transmittance plot and upon the transmittance of the solution has stabilised) and immediately analyzed for zeta potential. Additionally, at the end of the titration experiments, 50 mg of the filtered and dried precipitates were re-suspended in MilliQ® water, sonicated during 2 minutes for homogenization and dispersion of the AMC, and zeta potential measurements were immediately performed (six measurements within the

first two minutes, and two more three and five minutes after sonication, respectively), to ensure the robustness and representativeness of the results.

Theoretical electrical conductivity values (κ_{cal}) for the reaction solutions can be calculated following the protocol described in previous works (Ruiz-Agudo *et al*. 2017, 2021). In this work, the ionic molal conductivity (λ) of all ions was calculated using equation:

$$\lambda_i = \lambda_i^{\circ}(T) - \frac{A(T)I^{\frac{1}{2}}}{1+BI^{\frac{1}{2}}} \qquad Eq\ .S\text{-}1$$

where $\boldsymbol{\lambda_i^{\circ}}$ and *A* are functions of temperature (*T*, ºC), *B* is an empirical constant and *I* is the ionic strength of the solution. Equations for $\boldsymbol{\lambda_i^{\circ}}$ and *A* calculation and *B* values for different ions can be found in (McCleskey et al., 2012). *I*, which is a measure of the concentration of all charged ions in solution, can be calculated using:

$$I = \frac{1}{2}\sum m_i z_i^2 \qquad Eq.\ S\text{-}2$$

where z_i is the charge of the i^{th} ion. Since $\boldsymbol{\lambda_i^{\circ}}$ and *A* functions and *B* value for citrate are not available in the literature, and considering the dilute character of the solutions, we used the (constant) value of ionic molar conductivity reported in Lide (2004) as the ionic molal conductivity of citrate (210.6 mS kg cm^{-1} mol^{-1}).

This calculation gives higher κ_{cal} than the actual measured values (κ) (Fig. 1c), as a result of the ion clustering before nucleation:

$$\kappa = \kappa_{\mathrm{cal}} - c_{MgCO_3}\lambda_{\mathrm{MgCO_3}} \qquad Eq.\ S\text{-}4$$

where $\boldsymbol{c_{MgCO_3}}$ is the concentration of pre-nucleation $MgCO_3$ associates and $\boldsymbol{\lambda_{MgCO_3}}$ is the molal conductivity of $MgCO_3$ associates, estimated using the Kohlrausch law which considers that the molal conductivity of an electrolyte is given by the ionic molal conductivity of its components using the following equation:

$$\boldsymbol{\lambda_{MgCO_3} = \lambda_{Mg^{2+}} + n \cdot \lambda_{CO_3^{2-}}} \qquad Eq.\ S\text{-}5$$

where *n* is a dimensionless number corresponding to the ratio of anions to cations in the $MgCO_3$ prenucleation associates. The exact value of *n* can be determined by comparison with the concentration of pre-nucleation $MgCO_3$ associates determined from Mg activity measurements (*e.g*., Ruiz-Agudo *et al.*, 2017, 2021). However, such measurements were not reliable in our system under the experimental conditions selected since they were not able to show any decrease in free Mg^{2+} activity upon solid formation, detected from changes in conductivity and transmittance measurements. Considering n=1 as in the $CaCO_3$-H_2O system, $\boldsymbol{c_{MgCO_3}}$ was calculated (Fig. 1d) for control runs and solutions containing citrate. Calculations performed with *n* values of 2 and 3 led to similar trends, *i.e*. enhanced Mg^{2+} binding at the lower citrate concentration, less pronounced Mg^{2+} binding in PNCs for citrate > 0.1 mM (data not shown). Note that this calculation yields maximum concentration values, since Mg-binding by citrate is not considered.

Finally, 1 mL of the reaction media was drawn immediately before nucleation (indicated by the first steep fall in the solution transmittance, after ca. 1000 s and 2800 s for the control and 1 mM citrate solution, respectively -see black arrows in Fig. 1a in the main text-) and poured into a mixture of 75 % acetone and 25 % absolute ethanol contained in a plastic beaker that was afterwards sealed with Parafilm™. Drops of the resulting dispersion were deposited on carbon coated Cu grids prior to TEM observation using a FEI Titan, (300 kV) and a 30 µm objective aperture. A 10 µm aperture was used to obtained selected area electron diffraction (SAED) patterns from a circular area of a diameter ~0.2 µm. A Super X EDS detector (FEI) consisting of four SSD detectors with no window surrounding the sample was used to record compositional maps in STEM mode of representative areas of the samples, while STEM images were collected using a high-angle annular dark field (HAADF) detector.

Ex-situ analysis of precipitates.

Once the precipitation experiment was completed, the reaction media was filtered using Nucleopore membranes (ϕ = 200 nm) to separate the solids, which were subsequently analyzed by X-ray diffraction using a PANalytical X'Pert Pro X-ray diffractometer. Diffraction patterns were collected using Cu Kα radiation (λ = 1.5405 Å), from 3 to 50° 2θ range, at a scanning rate of 0.11° 2θ s^{-1}. Further characterisation was performed by Fourier Transform Infrared spectroscopy (FTIR) using an ATRproONE-FTIR spectrometer from Jasco (Model 6600) in the frequency range 400-4000 cm^{-1}, with a resolution of 2 cm^{-1} and 100 accumulations, and thermogravimetry and differential scanning calorimetry (TGA/DSC;) with a Mettler-Toledo TGA/DSC equipment in the temperature range 25-950 °C, at a heating rate of 10 K/min, with flowing air at 120 mL/min.

Supplementary Figures

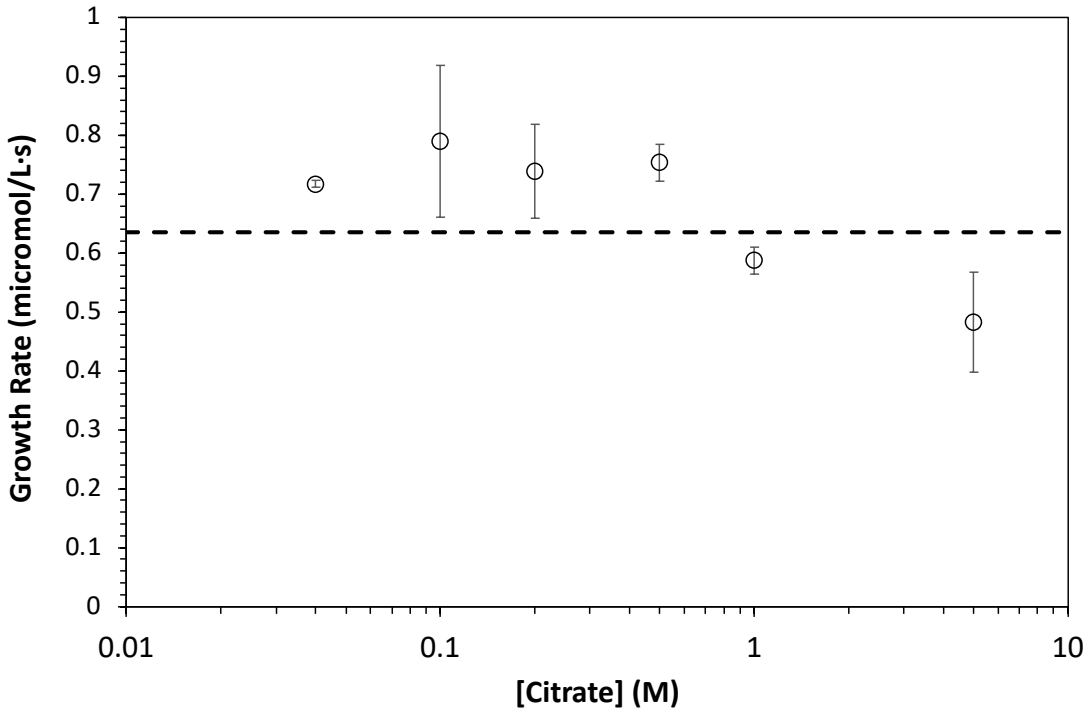

Figure S-1 AMC growth rate *vs.* citrate concentration determined from conductivity measurements as the ratio of the difference between theoretical and experimental conductivity and the molar specific conductivity of $MgCO_3$, assuming a 1:1 Mg^{2+} to CO_3^{2-} ratio in the solid. The dotted horizontal line represents the growth rate determined in the absence of citrate.

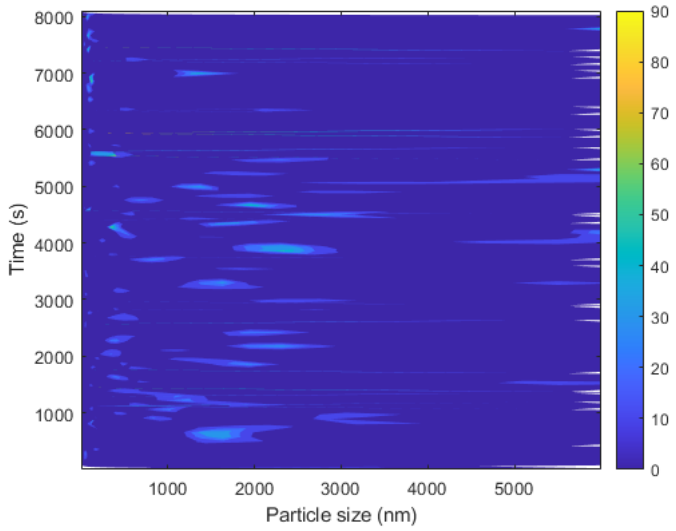

Figure S-2 Size evolution of the different (pre- and post-nucleation) species formed during titration experiments obtained by *in situ* dynamic light scattering (DLS) in the presence of 5 mM citrate.

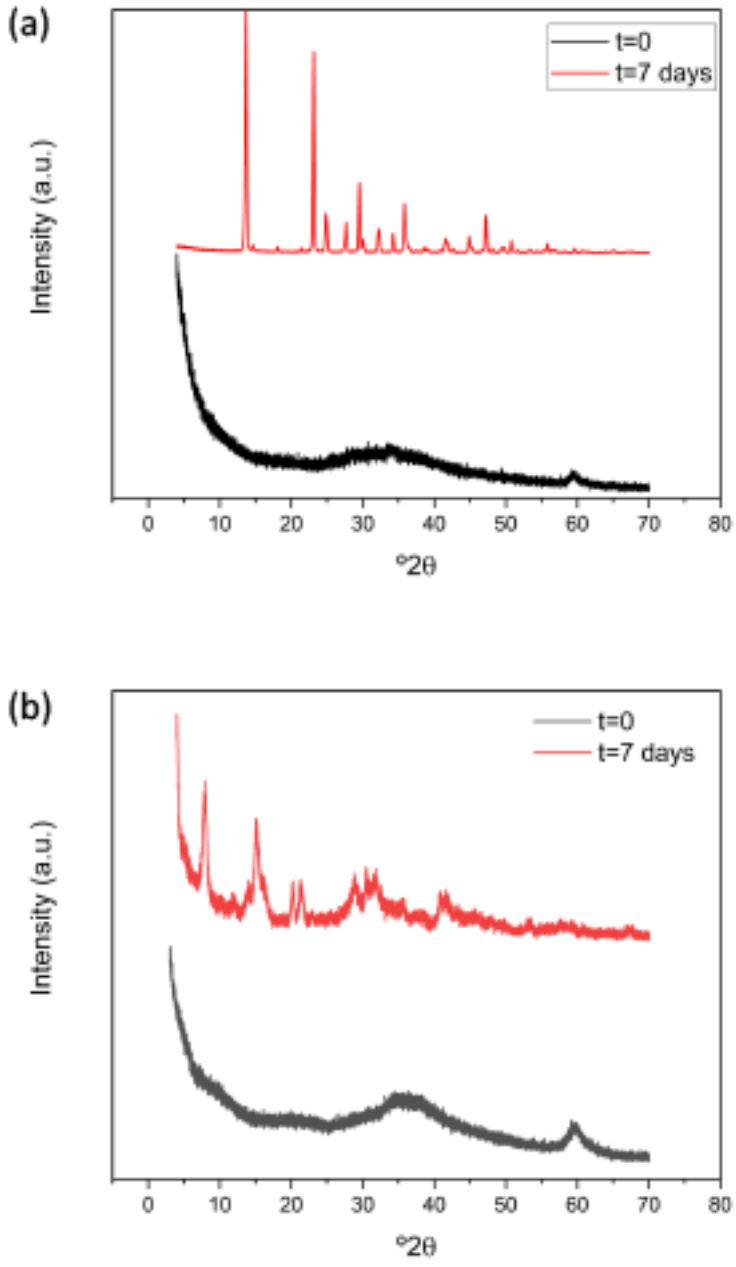

Figure S-3 XRD pattern of precipitates formed immediately after titration experiments (black plot) and after one week in the reaction media under constant stirring at 25 ºC (red plot). The absence of any diffraction peaks in the precipitates formed immediately after cessation of $MgCl_2$ dosing (black lines) confirms their amorphous nature. After one week, the precipitates are crystalline. In control runs (a), the main phase found was nesquehonite, while in 1 mM citrate solution the main crystalline phase formed was dypingite.

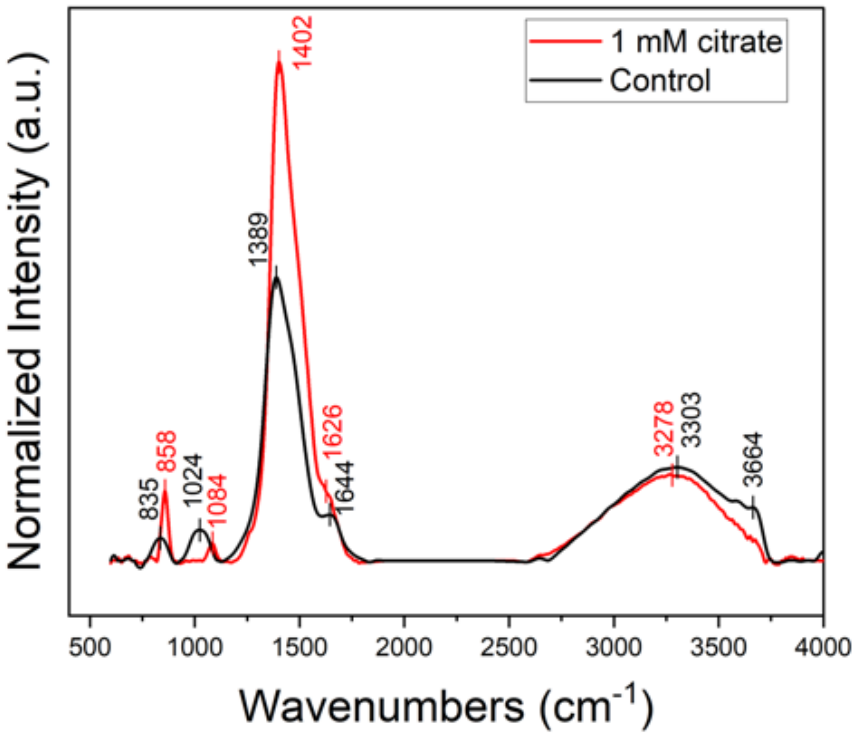

Figure S-4 FTIR spectra of AMC precipitates formed in control (black curve) and sodium citrate (1 mM, red curve) titration runs.

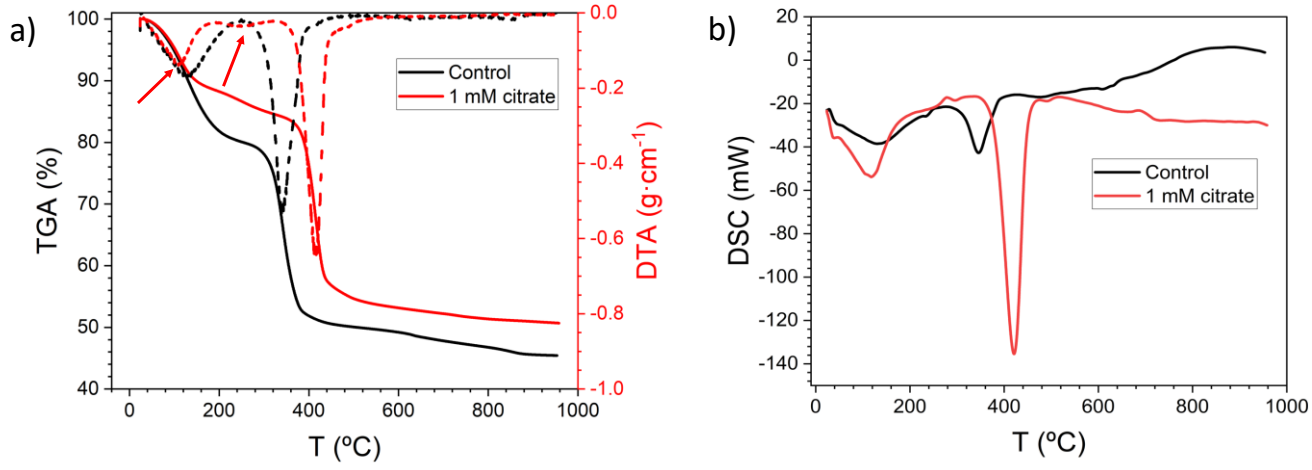

Figure S-5 TGA/DTA **(a)** and DSC **(b)** plots of the precipitates formed in titration runs. Red arrows mark the two dehydration steps observed in the case of citrate-bearing AMC (see main text for further explanation).

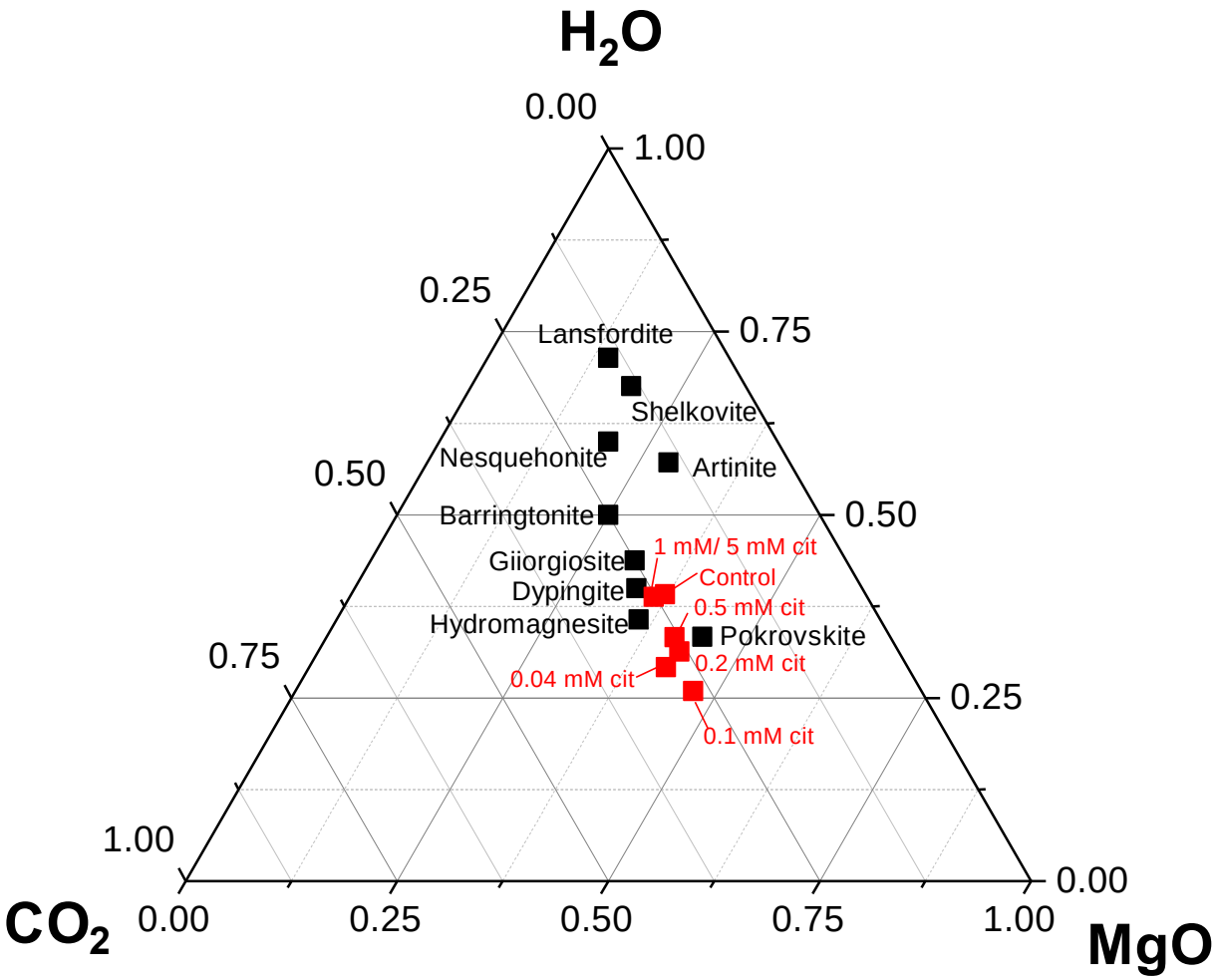

Figure S-6 Ternary phase diagram of the CO_2-MgO-H_2O system, showing hydrated magnesium carbonate minerals (black squares) and AMC samples synthesised in this work (red squares).

Supplementary Tables

	Zeta potential (mV)
AMC control 2010 s	-7.91 ± 0.33
AMC control 15000 s	-5.80 ± 0.16
AMC 5mM citrate 20000s	-3.93 ±0.40
AMC control redispersed in water	-8.54 ± 0.38
AMC 5mM citrate redispersed in water	-6.09 ± 0.51

Table S-1 Zeta potential values of control and citrate-bearing AMC. The values in the first three rows correspond to measurements of aliquots of the reaction medium with dispersed AMC particles collected at different elapsed times during titration. The values in the last two rows correspond to AMC samples dried and redispersed in MilliQ water.

Supplementary Information References

Lide, D.R. (Ed.). (2004) CRC handbook of chemistry and physics (85th ed.). CRC Press LLC, BocaRaton, FL. 2712 pp.

McCleskey, R.B., Nordstrom, D.K., Ryan, J.N., Ball, J.W. (2012) A new method of calculating electrical conductivity with applications to natural waters. *Geochimica et Cosmochimica Acta* 77, 369-382. https://doi.org/10.1016/j.gca.2011.10.031

Ruiz-Agudo, E., Burgos-Cara, A., Ruiz-Agudo, C., Ibáñez-Velasco, A., Cölfen, H., Rodriguez-Navarro, C. (2017) A non-classical view on calcium oxalate precipitation and the role of citrate. *Nature Communications* 8, 1-10. https://doi.org/10.1038/s41467-017-00756-5

Ruiz-Agudo, E., Ruiz-Agudo, C., Di Lorenzo, F., Alvarez-Lloret, P., Ibanez-Velasco, A., Rodriguez-Navarro, C. (2021) Citrate Stabilizes Hydroxylapatite Precursors: Implications for Bone Mineralization. *ACS Biomaterials Science & Engineering* 7, 2346-2357. https://doi.org/10.1021/acsbiomaterials.1c00196